Title: High resolution imaging and interpretation of three-dimensional RPE sheet structure

Authors: Kevin J. Donaldson[1], Jeffrey H. Boatright[1,2], John M. Nickerson[1]

Affiliations:

[1]Department of Ophthalmology, Emory University, Atlanta, Georgia, United States

[2]Atlanta Veterans Administration Center for Visual and Neurocognitive Rehabilitation, Decatur, Georgia, United States

Correspondence to: Dr. John M. Nickerson; Department of Ophthalmology, Emory University, B5602, 1365B Clifton Road, NE, Atlanta, GA, 30322; Phone 404-778-4411; email: litjn@emory.edu

Funding: Supported by National Institutes of Health (NIH) grants R01EY028450, R01EY021592, P30EY006360, R01EY028859, T32EY07092, the Abraham and Phyllis Katz Foundation, VA RR&D I01RX002806 and I21RX001924, VA RR&D C9246C (Atlanta Veterans Administration Center for Excellence in Vision and Neurocognitive Rehabilitation), and a Challenge Grant to the Department of Ophthalmology at Emory University from Research to Prevent Blindness, Inc.

Conflict of Interest Statement: None of the authors has a conflict of interest.

Keywords: Retinal Pigment Epithelium; RPE; 3D reconstruction; cell segmentation; EMT; multinucleation; blood-retina barrier

Abstract

The retinal pigment epithelium (RPE) is a monolayer of pigmented cells which plays an essential role in visual function via its interaction with the adjacent neural retina. Typically hexagonal in shape and arranged in a mosaic-like pattern, RPE cells maintain a relatively uniform size and arrangement in healthy eyes. Under stress or disease conditions such as age-related macular degeneration (AMD) and other heritable vision disorders, individual RPE cell dysmorphia has been observed. This has led to investigation of potential cellular compensatory mechanisms which may be dysregulated, affecting proper barrier structure and function. A commonly observed dysmorphic trait is that of enlarged cells which appear to be multinucleated (containing more than two nuclei) when viewed in two-dimensional (2D), immunohistochemically labeled images from the apical surface perspective. One explanation for the multinucleation is that of ongoing cellular fusion which the RPE may be employing to maintain cell-to-cell contact while simultaneously conserving cellular resources in unhealthy tissue. While this may be the most likely interpretation, caution should be applied when interpreting traditional (2D) images which only use cell border outline markers in the absence of lateral markers. Here we present two examples of high-resolution confocal images which allow for three-dimensional (3D) viewing of a traditional apical border delineation marker (ZO-1) and nuclei as well as labeling of alpha catenin which can serve as a lateral cell membrane marker. We find multiple examples in two separate RPE damage models where enlarged, seemingly multinucleate, cells are in actuality not multinucleate and instead appear this way due to surrounding cell nuclei and lateral cell membrane displacement towards the central cell. When viewed from the apical surface, these nuclei appear contained by the ZO-1 border, however when viewed from multiple angles it becomes apparent that this is not the case. This approach calls for more careful analyses in future studies investigating RPE sheet dysmorphia as this could lead to potential misinterpretation of the multinucleation phenomenon and by extension, the potential underlying fusion mechanism.

Introduction

The retinal pigment epithelium (RPE) is a monolayer sheet of cells in the eye, forming a barrier between the neural retina and the choroid in the eye. The RPE plays a critical role in retinal homeostasis through a myriad of functions, primarily servicing the adjacent rod and cone photoreceptor cells of the neural retina (Bhatia et al., 2016; Rashid et al., 2016; Wang et al., 2018; Zhang et al., 2019)(Strauss, 2005).

In healthy RPE tissue, the apical surfaces of individual cells in the sheet present with the appearance of regular hexagons when viewed *en face*. Each RPE cell typically makes contact with six immediately adjacent neighbor RPE cells, establishing the outer blood retina barrier. RPE cells are terminally differentiated and no longer divide in both adult human subjects and rodent model species.

Studies examining RPE cell structure have revealed correlations between abnormal morphology and multiple aging and blindness disorders, such as age-related macular degeneration (AMD) and other inherited retinopathies (Marmor & Wolfensberger, 1998; Gambril et al., 2019; Bonilha, 2008; Christensen et al., 2017; Michaelides et al., 2003). Under stressful conditions the RPE sheet, which is generally highly robust, can undergo numerous signs of damage, exhibiting both functional and morphological changes. While the RPE sheet can lose barrier functions, it appears to go to great lengths to preserve the monolayer barrier by employing multiple reconfiguration processes. For instance, dead or dying RPE cells can be extruded in a classical purse-string mechanism, and surrounding cells appear to fill in by changing shapes in a pie-like pattern.

Under aging conditions, as well as after severe stress, some of the cells can become much larger, but it is unclear how this happens. Is it a single cell that gains size, or possibly two cells fused together, resulting in a larger single cell? Additionally, it is unclear how these stressed or damaged cells are able to move. Is there a modification to Bruch's membrane itself such that cells translocate by traversing laterally on the surface of a stationary Bruch’s membrane, or if it is the other way around where perhaps Bruch’s membrane is modified itself and the attached anchored cells move as the membrane does.

An additional observation of these cells under abnormal conditions is that some of the cells appear to be multinucleate. While it is well established that rodent RPE cells may have either one nucleus or two nuclei per cell, it is less clear if, or how, a single RPE cell might acquire additional nuclei beyond two. It could be that due to movement over the top or underneath another RPE cell might look like there are 3 or more nuclei in a

single RPE cell, but in fact, due to parallax in standard *en face* imaging techniques, it just looks like there are multiple nuclei per RPE cell. On the other hand, pathological circumstances might lead to cell fusion, which may offer cells the opportunity to share resources and thus save the remaining damaged cells. Cell fusion may also be a potential mechanism which could enable thinner cells to cover more of Bruch's membrane via an increase in surface area without requiring an increase in cell number. There is good evidence to support this model in aging and potential stress models (Chen et al., 2016), thus it becomes important to ensure that we accurately identify which nuclei belong to which cell and whether or not multinucleate cells are true hallmarks of abnormal RPE sheet or potential imaging artifact.

A potential confound of visual RPE nuclei localization in standard *en face* images is that the choroid has many nucleated cells. Show-through of endothelial cells can occur if the density of pigment granules of the RPE or melanocytes is low, which might occur in disease and therefore it is essential that we do not mistakenly count any of these nuclei when determining RPE nuclei counts per cell. Thus, it is critical to accurately observe the location and shape of nuclei in order to establish whether a given nucleus is really a nucleus of the RPE or another confounding layer in a flatmount.

Standard imaging of *ex vivo* RPE sheet preparations typically involves simultaneous immunofluorescent staining of apical cell border proteins, such as ZO-1, and nuclei with different wavelength fluorophores. Images acquired with a confocal microscope are usually at a lower magnification (10-20x objective) as global patterning is of initial interest in multifield stitched images. In some experiments, multiple images in the z-axis are acquired (z-stacks) which are then converted to 2D maximum intensity projections (MIPs) by collapsing the z-axis and forcing a straight apical to basal orientation of RPE cells. This process can introduce the aforementioned parallax as nuclei from adjacent cells can actually appear within the cell border of a central cell if enlarged at only the apical surface, and not uniformly throughout the z-axis.

While some 3D ultrastructure imaging of RPE cells has been achieved via serial block face scanning electron microscopy (SBF-SEM)(Keeling et al., 2020), this method still presents a technical barrier for many labs as well as not being suited for simultaneous whole eye image acquisition used in disease phenotyping.

A high magnification (60x) 3D rendering of the RPE sheet with fluorescent staining of the apical cell borders, basal, and lateral faces of individual RPE cells can help us decode patterns associated with normal RPE cell properties, as well as those in stressed or damaged conditions. Additionally, when imaged with

modern, automated confocal microscopes, entire eye flatmount preps can be obtained for large scale pattern recognition before subsequent imaging of specific dysmorphic cells of interest.

We and others find that RPE cells undergo progressive degeneration in patients (Bhatia et al., 2016; Rashid et al., 2016; Wang et al., 2018; Q. Zhang et al., 2019) and in animal models of retinal damage or disease (Cano et al., 2014; Chrenek et al., 2012; N. Zhang et al., 2021), exhibiting characteristics of dedifferentiation reminiscent of epithelial-to-mesenchymal transition (EMT; reviewed in Datta et al., 2017). Experiments with cultures of RPE cells or explants also show that when stressed, RPE cells appear to dedifferentiate via EMT-like processes (Cano et al., 2014; Datta et al., 2017, 2023; Mertz et al., 2021; Sripathi et al., 2023; Sripathi, Hu, Liu, et al., 2021; Sripathi, Hu, Turaga, et al., 2021)(22,54-59).

RPE epithelial-to-mesenchymal transition" (RPE EMT) may imply that RPE cells lose apical-basal polarity, normal intercellular adhesion, and outer blood-retina barrier functions. RPE cells might become mesenchymal cells because they have begun to move and migrate and invade the neural retina. This transition might include the loss of E- and P-cadherin and increase expression of putative "mesenchymal markers" including SMA, Vimentin, Snail, Twist, Slug.

“RPE EMT” may simply be a wound healing response, but it likely includes fibrosis. Whatever the process, it is proposed that it is triggered by external signals, including growth factors, cytokines, and extracellular matrix components. Whether "RPE EMT" is a true EMT, it may share commonalities with other forms of EMT; and drugs that affect other EMT forms might turn out to be effective in RPE disease and wound healing

Methods

Animal models of RPE damage

All mouse handling procedures and care were approved by the Emory Institutional Animal Care and Use Committee and followed the ARVO Statement for the Use of Animals in Ophthalmic and Vision Research. Adult (postnatal day 90) male C57BL6/J mice were obtained from Charles River Laboratory (Wilmington, MA, USA) and were housed under a 12:12-hour light–dark cycle. Following our previously published protocol (Chrenek et al., 2016), one mouse was exposed to toxic levels of light which caused light-induced retinal degeneration (LIRD). In a second mouse, a subretinal injection surgery was performed, causing a temporary

retinal detachment and subsequent RPE sheet disruption (Donaldson et al., 2018). Both animals were sacrificed and tissue harvested a few days after the respective procedures.

Tissue preparation and fluorescent labeling

Whole eye RPE flatmounts (FMs) were prepared following our previously published protocols (Boatright et al., 2015; Jiang et al., 2013) with some minor modifications. Eyes were fixed in Z-Fix (Anatech Ltd, Battle Creek, MI, USA) for 10 min, and then washed three times with Hank's Balanced Salt Solution (HBSS; Cat. #14025092, Gibco by Life Technologies, Grand Island, NY, USA). Eyes were stored at 4°C for up to 24 hours before being dissected. Following the removal of the iris and neural retina, four radial cuts were made to produce four RPE–scleral flaps with additional smaller relief cuts to aid with flattening of the tissue. FMs were then mounted RPE side up, on conventional microscope slides to which a silicon gasket had been applied (Grace Bio-Labs, Bend, OR, USA).

The FMs were rinsed with HBSS, then incubated in blocking buffer consisting of 1% BSA (Sigma, St. Louis, MO, USA) in 0.1% Triton X-100 (Sigma) HBSS solution for 1 hour at room temperature. Primary incubation occurred overnight at room temperature (1:100 anti-ZO-1, Cat. #MABT11, MilliporeSigma; 1:500 anti-CTNNA1 (alpha-catenin), Cat. #EP1793Y, Abcam, Cambridge, MA, USA). Following washes with 0.1% Triton-X-100 in HBSS, FMs were incubated with secondary antibodies (Alexa Fluor 488,1:1000 donkey anti-rat immunoglobulin G, Cat. #A21208, Thermo Fisher Scientific, Waltham, MA, USA; Alexa Fluor 568, 1:1000 goat anti-rabbit immunoglobulin G, Cat. #A11036, Thermo Fisher Scientific) overnight at room temperature. FMs were washed with Hoechst 33258 nuclear stain in 0.1% Triton X-100 in HBSS three times, followed by two washes with only wash buffer, and then mounted with Fluoromount-G (Cat. #17984-25, Electron Microscopy Sciences, Signal Hill, CA, USA), coverslipped, and allowed to set overnight.

Confocal microscopy and 3D image visualization

Whole eye FMs were imaged in their entirety at lower magnification (10x objective lens) using a Nikon Ti microscope with C1 confocal scanner (Nikon Instruments Inc., Melville, NY, USA), with sufficient z-stack thickness to capture entire RPE cells throughout the FM. Regions of interest (ROIs) containing dysmorphic cells were then reimaged at higher magnification (60x and 100x objective lenses) with appropriate z-slice spacing to satisfy the Nyquist requirement for 3D capture and viewing. Imaris (version 8.4, Bitplane, Oxford,

UK) software was used to isolate and post-process ROIs from raw confocal files as well as generate videos highlighting cell membrane, internal alpha-catenin structure and nuclear position from multiple viewing angles.

Results

We present images, reconstructions, and videos generated from high magnification confocal z-stacks of two damage-model RPE sheets highlighting 3D ultrastructure of individual cells. Specifically, we selected ROIs that exhibit a heterogenous mix of normal and dysmorphic cells and include larger than normal, multinucleate cells (**Fig 1** and **Vid 1 and 2**). Extending the visualization of conventionally sectioned ocular tissue, we also present 3D images, reconstructions and videos of lateral and basal RPE cell surfaces (**Fig 2**, **Vid 3**). Finally, we show both local and global disruptions in the RPE sheet reminiscent of EMT in entire mouse eyes following induced RPE loss via intravenous NaIO3 injections (**Fig 4** and **5**).

Video 1 presents an isolated z-stack imaged at 100x magnification with labeling of ZO-1 (green), alpha catenin (red), and nuclei (blue) from a LIRD-damaged whole-eye RPE FM. Initially oriented basal-side up, with the apical surface away from the viewer, a large, seemingly multinucleate cell is found in the top-middle of the image. The cell is much larger than normal by about 3-fold on each of the X- and Y-axes, suggesting an 8-10-fold increase in cell size. This cell has a number of nuclei around its perimeter which appear to be within the cell depending on viewing angle. Additionally, there is a large auto-fluorescent aggregate (appearing as yellow here) of unknown composition, which is hypothesized to be internalized rod/cone outer segments or lipofuscin, contained within the cell. Other cells of interest include those at the bottom middle, where again it appears that larger cells are multinucleated with a number of nuclei appearing near their perimeters. As playback proceeds, orientation is flipped with the apical surface being at the top when viewed orthogonally and closest to the viewer later when viewed *en face*. The viewer is then “flown” through the image where the auto fluorescent aggregate and laterally oriented alpha catenin is visible below the apically located ZO-1 rim. Zooming closer and viewing from the apical surface, reveals multiple nuclei clustered around the perimeter of the enlarged cell. The alpha catenin signal is removed to highlight the ZO-1 outline, mimicking typical RPE cell border delineation imaging. When the alpha catenin channel is restored, it is apparent that the large cell is overhanging these nuclei on the ring and edge. When rotated to a side or underneath view, it becomes clear that these nuclei

actually belong not to the central cell but to the adjacent neighboring cells and have been pushed outward in a slightly bulging cell wall. We do not know yet whether it is the central large cell pushing over the top of the adjacent neighbors or if the neighbors are pulling on the central cell resulting in over-coverage of the neighboring cells.

Video 2 presents a 3D view of a region which contains greatly dysmorphic RPE cells following SRI-induced retinal detachment and recovery. Here, relying on ZO-1 (green) solely for individual cell demarcation (as is typically found in the field) is problematic as abnormally large cells are adjacent to select cells of strikingly smaller area. This “purse-string” pattern has been observed in multiple models of RPE stress when viewed in *en face* 2D images and potentially reflects cells in the process of programmed cell death and/or removal from the sheet. However, it is unclear if the larger cells are actively pushing out the smaller cells or merely expanding to fill in the previously occupied space to maintain the RPE’s barrier integrity. When imaged with concurrent alpha catenin staining (red), the viewer can observe many different underlying cellular shapes which don’t directly align with the ZO-1 perimeter staining. For instance, in the top middle of the video, there is a large, spherical structure of labeled alpha catenin which spreads underneath multiple ZO-1 delineated perimeters. This structure encompasses two nuclei (blue), separating them from the pair of nuclei directly below. Without this additional ultrastructural information, the viewer might erroneously conclude that all four nuclei are contained in an enlarged, multinucleate cell, when in reality it is two adjacent cells. When looking at the enlarged cell in the right-middle region of the video (just below the ZO-1 labeled cell of very small area), the viewer appears to see four nuclei encompassed by the ZO-1 perimeter. However, when viewed as a 3D aspect, it is apparent that the left pair of nuclei are visible through an open cylinder of alpha catenin, suggesting that they are located in a different cell, with the pair on the right more superficially separated. Special care should be taken to determine in 3D space if these two pair of nuclei are contained by the enlarged cell or are indeed in separate cells. Thus, when viewed in 3D with the addition of lateral labeling, this video exemplifies the multitude of dynamic and dysmorphic reorganization that occurs following RPE stress.

Conclusions

The images and work presented here emphasize the need to determine the location of nuclei accurately, precisely, and reliably in RPE cells. By using relatively standard confocal microscopy but with the appropriate approach to instrumentation and image acquisition settings, we simply employ a careful look at nuclear localization in 3D. We used a user-friendly, and commercially available program, Imaris, for visualization and creation of videos, however other software (including ImageJ with appropriate plugins) would surely be adequate for the same purpose.

A key question when analyzing RPE dysmorphia is if neighboring cell nuclei remain in their respective origin cells but are visualized within an enlarged central cell's borders when viewed *en face*, or are indeed components of a larger multinucleate cell. Our results suggest that when looking at large, multinuclear cells in a RPE sheet which has been subjected to stress, it is important to visualize these changes from a 3D perspective at the individual cell level. In multiple images, we show that nuclei which appear as members of a large multinucleate cell are actually still members of surrounding cells when viewed at higher magnification and alternate angles than the standard apical to basal collapsed view.

Correct interpretation of multiple nuclei in RPE cells depends on a better understanding of how the basal and lateral faces of the RPE cells move following aging and stress. A small proportion of RPE cells appear capable of greatly increasing in size following severe stress. Largely absent under normal conditions, it remains unclear if all RPE cells have this capability to vastly enlarge, or if only a small subclass of RPE cells can do this. Further experiments investigating damage-associated morphological abnormalities are required to understand the unusually large cell phenotype and find potential common traits, if any, between damage conditions. It is likewise unclear if these cells can undergo further morphological or functional transformations such as, but not limited to, epithelial–mesenchymal transition (EMT).

References

Bhatia, S. K., Rashid, A., Chrenek, M. A., Zhang, Q., Bruce, B. B., Klein, M., Boatright, J. H., Jiang, Y., Grossniklaus, H. E., & Nickerson, J. M. (2016). Analysis of RPE morphometry in human eyes. *Molecular Vision*, *22*, 898–916.

Boatright, J. H., Dalal, N., Chrenek, M. A., Gardner, C., Ziesel, A., Jiang, Y., Grossniklaus, H. E., & Nickerson, J. M. (2015). Methodologies for analysis of patterning in the mouse RPE sheet. *Molecular Vision*, *21*, 40–60.

Bonilha, V. L. (2008). Age and disease-related structural changes in the retinal pigment epithelium. *Clinical Ophthalmology*, *2*(2), 413–424. https://doi.org/10.2147/opth.s2151

Cano, M., Wang, L., Wan, J., Barnett, B. P., Ebrahimi, K., Qian, J., & Handa, J. T. (2014). Oxidative stress induces mitochondrial dysfunction and a protective unfolded protein response in RPE cells. *Free Radical Biology & Medicine*, *69*, 1–14. https://doi.org/10.1016/j.freeradbiomed.2014.01.004

Chen, M., Rajapakse, D., Fraczek, M., Luo, C., Forrester, J. V., & Xu, H. (2016). Retinal pigment epithelial cell multinucleation in the aging eye – a mechanism to repair damage and maintain homoeostasis. *Aging Cell*, *15*(3), 436. https://doi.org/10.1111/acel.12447

Chrenek, M. A., Dalal, N., Gardner, C., Grossniklaus, H., Jiang, Y., Boatright, J. H., & Nickerson, J. M. (2012). Analysis of the RPE sheet in the rd10 retinal degeneration model. *Advances in Experimental Medicine and Biology*, *723*, 641–647. https://doi.org/10.1007/978-1-4614-0631-0_81

Chrenek, M. A., Sellers, J. T., Lawson, E. C., Cunha, P. P., Johnson, J. L., Girardot, P. E., Kendall, C., Han, M. K., Hanif, A., Ciavatta, V. T., Gogniat, M. A., Nickerson, J. M., Pardue, M. T., & Boatright, J. H. (2016). Exercise and Cyclic Light Preconditioning Protect Against Light-Induced Retinal Degeneration and Evoke Similar Gene Expression Patterns. *Advances in Experimental Medicine and Biology*, *854*, 443–448. https://doi.org/10.1007/978-3-319-17121-0_59

Christensen, D. R. G., Brown, F. E., Cree, A. J., Ratnayaka, J. A., & Lotery, A. J. (2017). Sorsby fundus dystrophy – A review of pathology and disease mechanisms. *Experimental Eye Research*, *165*, 35–46. https://doi.org/10.1016/j.exer.2017.08.014

Datta, S., Cano, M., Ebrahimi, K., Wang, L., & Handa, J. T. (2017). The impact of oxidative stress and inflammation on RPE degeneration in non-neovascular AMD. *Progress in Retinal and Eye Research*, *60*, 201–218. https://doi.org/10.1016/j.preteyeres.2017.03.002

Datta, S., Cano, M., Satyanarayana, G., Liu, T., Wang, L., Wang, J., Cheng, J., Itoh, K., Sharma, A., Bhutto, I., Kannan, R., Qian, J., Sinha, D., & Handa, J. T. (2023). Mitophagy initiates retrograde mitochondrial-nuclear signaling to guide retinal pigment cell heterogeneity. *Autophagy*, *19*(3), 966–983. https://doi.org/10.1080/15548627.2022.2109286

Donaldson, K. J., Skelton, H. M., Sellers, J. T., Grossniklaus, H., & Nickerson, J. M. (2018). Novel ex and in vivo methods for non-invasive longitudinal tracking of RPE dysmorphology following subretinal injections. *Investigative Ophthalmology & Visual Science*, *59*(9), 4982.

Gambril, J. A., Sloan, K. R., Swain, T. A., Huisingh, C., Zarubina, A. V., Messinger, J. D., Ach, T., & Curcio, C. A. (2019). Quantifying Retinal Pigment Epithelium Dysmorphia and Loss of Histologic Autofluorescence in Age-Related Macular Degeneration. *Investigative Ophthalmology & Visual Science*, *60*(7), 2481–2493. https://doi.org/10.1167/iovs.19-26949

Jiang, Y., Qi, X., Chrenek, M. A., Gardner, C., Boatright, J. H., Grossniklaus, H. E., & Nickerson, J. M. (2013). Functional Principal Component Analysis Reveals Discriminating Categories of Retinal Pigment Epithelial Morphology in Mice. *Investigative Ophthalmology & Visual Science*, *54*(12), 7274–7283. https://doi.org/10.1167/iovs.13-12450

Keeling, E., Chatelet, D. S., Tan, N. Y. T., Khan, F., Richards, R., Thisainathan, T., Goggin, P., Page, A., Tumbarello, D. A., Lotery, A. J., & Ratnayaka, J. A. (2020). 3D-Reconstructed Retinal Pigment Epithelial Cells Provide Insights into the Anatomy of the Outer Retina. *International Journal of Molecular Sciences*, *21*(21), Article 21. https://doi.org/10.3390/ijms21218408

Marmor, M. F., & Wolfensberger, T. J. (1998). The retinal pigment epithelium. In *Function and Disease* (pp. 103–134). https://medtextfree.wordpress.com/2010/12/29/chapter-100-retinal-pigment-epithelium/

Mertz, J. L., Sripathi, S. R., Yang, X., Chen, L., Esumi, N., Zhang, H., & Zack, D. J. (2021). Proteomic and phosphoproteomic analyses identify liver-related signaling in retinal pigment epithelial cells during EMT. *Cell Reports*, *37*(3), 109866. https://doi.org/10.1016/j.celrep.2021.109866

Michaelides, M., Hunt, D. M., & Moore, A. T. (2003). The genetics of inherited macular dystrophies. *Journal of Medical Genetics*, *40*(9), 641–650. https://doi.org/10.1136/jmg.40.9.641

Rashid, A., Bhatia, S. K., Mazzitello, K. I., Chrenek, M. A., Zhang, Q., Boatright, J. H., Grossniklaus, H. E., Jiang, Y., & Nickerson, J. M. (2016). RPE Cell and Sheet Properties in Normal and Diseased Eyes. In C. Bowes Rickman, M. M. LaVail, R. E. Anderson, C. Grimm, J. Hollyfield, & J. Ash (Eds.), *Retinal Degenerative Diseases* (pp. 757–763). Springer International Publishing. https://doi.org/10.1007/978-3-319-17121-0_101

Sripathi, S. R., Hu, M.-W., Liu, M. M., Wan, J., Cheng, J., Duan, Y., Mertz, J. L., Wahlin, K. J., Maruotti, J., Berlinicke, C. A., Qian, J., & Zack, D. J. (2021). Transcriptome Landscape of Epithelial to Mesenchymal Transition of Human Stem Cell-Derived RPE. *Investigative Ophthalmology & Visual Science*, *62*(4), 1. https://doi.org/10.1167/iovs.62.4.1

Sripathi, S. R., Hu, M.-W., Turaga, R. C., Mertz, J., Liu, M. M., Wan, J., Maruotti, J., Wahlin, K. J., Berlinicke, C. A., Qian, J., & Zack, D. J. (2021). Proteome Landscape of Epithelial-to-Mesenchymal Transition (EMT) of Retinal Pigment Epithelium Shares Commonalities With Malignancy-Associated EMT. *Molecular & Cellular Proteomics: MCP*, *20*, 100131. https://doi.org/10.1016/j.mcpro.2021.100131

Sripathi, S. R., Hu, M.-W., Turaga, R. C., Mikeasky, R., Satyanarayana, G., Cheng, J., Duan, Y., Maruotti, J., Wahlin, K. J., Berlinicke, C. A., Qian, J., Esumi, N., & Zack, D. J. (2023). IKKβ Inhibition Attenuates Epithelial Mesenchymal Transition of Human Stem Cell-Derived Retinal Pigment Epithelium. *Cells*, *12*(8), 1155. https://doi.org/10.3390/cells12081155

Strauss, O. (2005). The retinal pigment epithelium in visual function. *Physiological Reviews*, *85*(3), 845–881. https://doi.org/10.1152/physrev.00021.2004

Wang, J., Zibetti, C., Shang, P., Sripathi, S. R., Zhang, P., Cano, M., Hoang, T., Xia, S., Ji, H., Merbs, S. L., Zack, D. J., Handa, J. T., Sinha, D., Blackshaw, S., & Qian, J. (2018). ATAC-Seq analysis reveals a widespread decrease of chromatin accessibility in age-related macular degeneration. *Nature Communications*, *9*(1), 1364. https://doi.org/10.1038/s41467-018-03856-y

Zhang, N., Zhang, X., Girardot, P. E., Chrenek, M. A., Sellers, J. T., Li, Y., Kim, Y.-K., Summers, V. R., Ferdous, S., Shelton, D. A., Boatright, J. H., & Nickerson, J. M. (2021). Electrophysiologic and Morphologic Strain

Differences in a Low-Dose NaIO3-Induced Retinal Pigment Epithelium Damage Model. *Translational Vision Science & Technology*, *10*(8), 10. https://doi.org/10.1167/tvst.10.8.10

Zhang, Q., Chrenek, M. A., Bhatia, S., Rashid, A., Ferdous, S., Donaldson, K. J., Skelton, H., Wu, W., See, T. R. O., Jiang, Y., Dalal, N., & Nickerson, J. M. (2019). Comparison of histologic findings in age-related macular degeneration with RPE flatmount images. *Molecular Vision*.

Figures

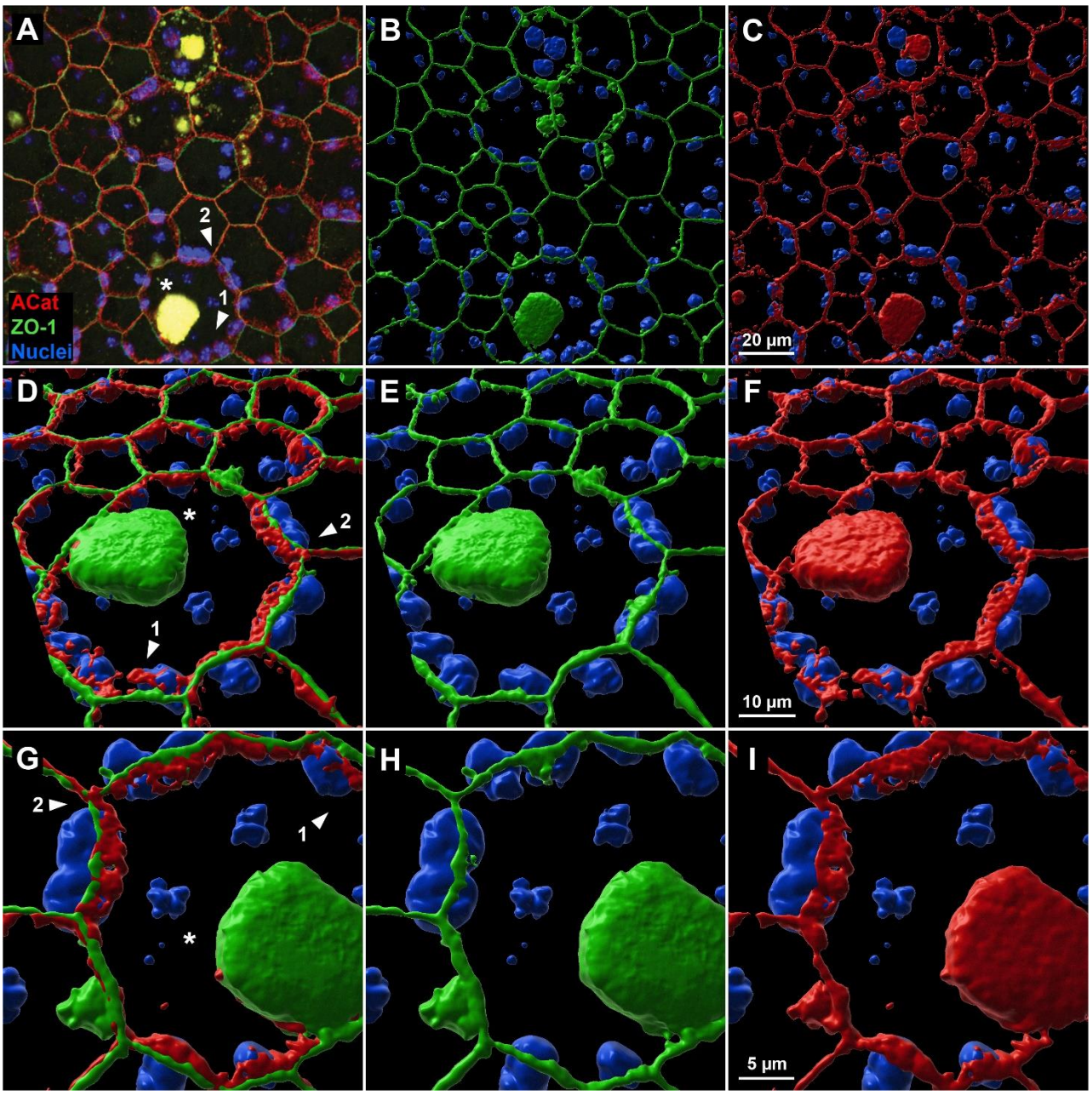

Figure 1 – 3D reconstruction of apical and lateral structure of single cells in RPE sheet following LIRD

(A) Original ROI selection from entire RPE-FM confocal image with labeling of cell perimeter marker ZO-1 (green), lateral surface and perimeter marker alpha catenin (red) and nuclei (blue). 3D reconstructions of the same ROI were made using IMARIS to show nuclear position in relation to ZO-1 **(B, E, H)** and alpha catenin **(C, F, I)** separately as well as combined **(D,G)**. Numbered arrows **(1, 2)** reference multinuclear clusters of interest which are then further visualized at increasing magnification. **Arrow 1** highlights an abnormally large RPE cell with apparent multinucleation in original 2D confocal image **(A)**. Higher magnification and alternate

viewing angles reveal instead that multiple nuclei are in highly lateralized positions of adjacent cells (also seen near **Arrow 2**). **Asterisk(*)** indicates auto fluorescent aggregate frequently found in LIRD-affected RPE tissue. **Video 1** provides additional viewing angles and magnification of this specific ROI.

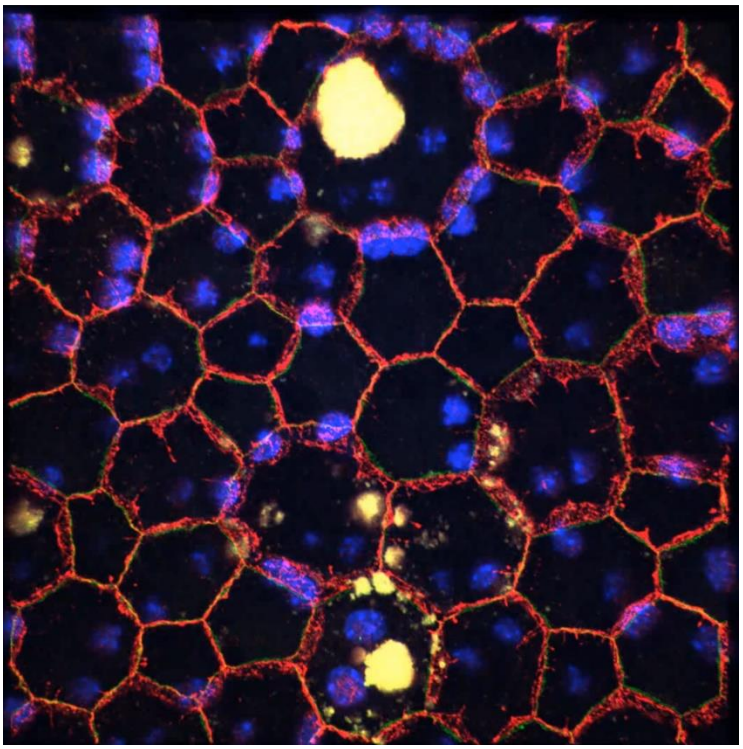

Video 1 – Multi-angle and magnification viewing of LIRD-affected RPE cells

3D video of confocal z-stack (100x magnification) showing ZO-1 cell perimeter (green), alpha catenin lateral and perimeter (red) and nuclear (blue) labeling from various angles not available in traditional 2D *en face* viewing from the apical surface. RPE cells have developed dysmorphia following LIRD. Large, seemingly multinucleate cells are shown to contain only a maximum of two nuclei when viewed from alternate angles and with concurrent lateral labeling of alpha catenin.

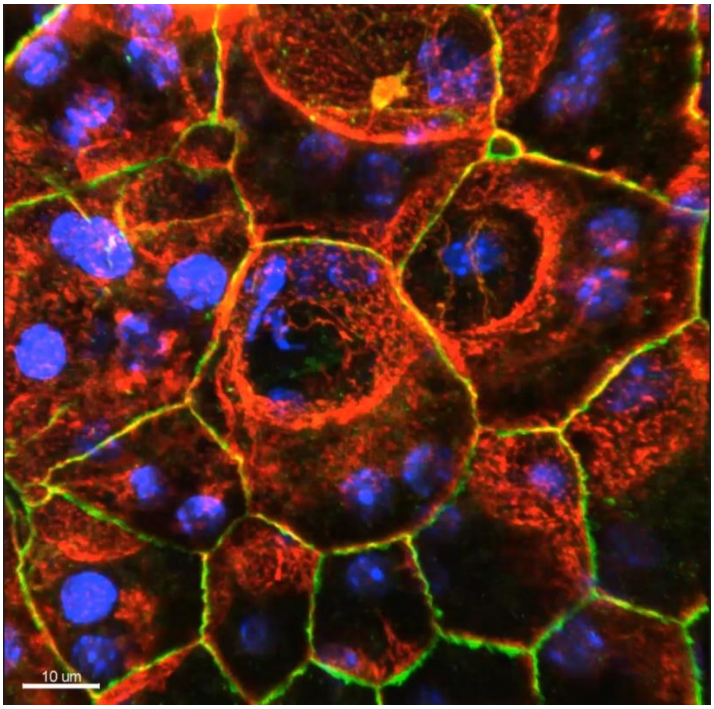

Video 2 – **Multi-angle view of RPE cell dysmorphia following SRI-induced retinal detachment.**

3D video of confocal z-stack (100x magnification) showing ZO-1 cell perimeter (green), alpha catenin lateral and perimeter (red) and nuclear (blue) labeling. Vast changes in individual RPE cell size, shape, orientation and alignment are visible during recovery from SRI-induced retinal detachment. Again, large, seemingly multinucleate cells are shown to contain less nuclei than expected when counted using ZO-1 perimeter staining and typical apical viewing, instead of lateral labeling of cell membranes and alternative viewing angles in 3D.

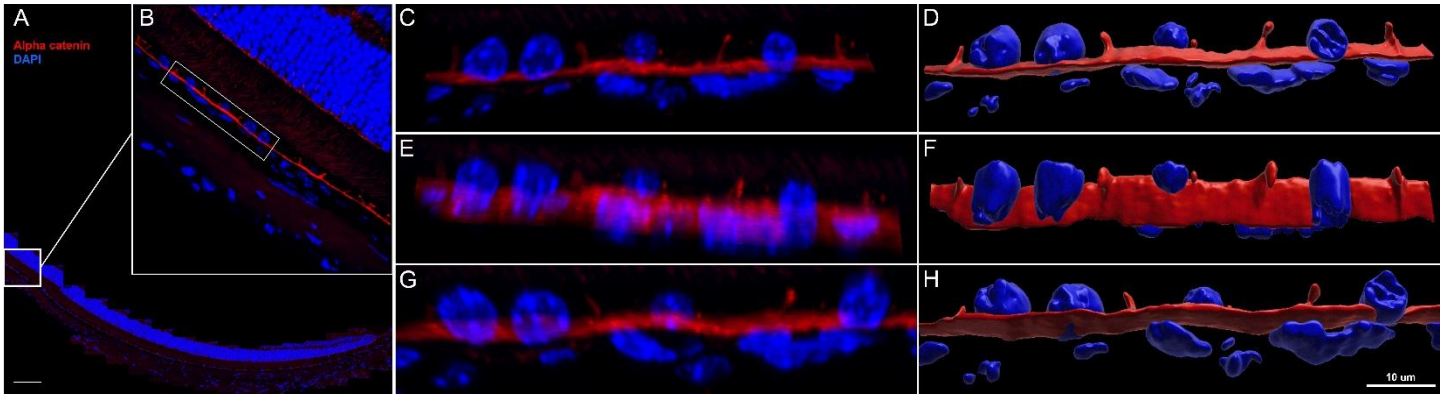

Figure 2 – Confocal images and corresponding 3D reconstruction of the retina-RPE-choroid with lateral and basal surface labeling of RPE cell membranes in normal mouse eyes.

(A, B) ROI selection from a 5 µm-thick cross-section labeled for alpha catenin (red) and nuclei (blue), scale bar = 100 µm. A 3-cell-wide region (bounding box in **B**) was isolated to provide alternate-angle views **(C, E, G)** and corresponding 3D reconstructions **(D, F, H)**. C and D are lateral views showing distinct morphologies in RPE nuclei (5 µm, round/potato shapes, 5-6 speckles) versus choriocapillaris nuclei (axially thin, irregular, less speckling). Alpha catenin labels lateral and basal faces with uniform staining and thickness. Lateral RPE walls show no clear orientation pattern in adjacent cells with angling > 45° relative to basal surfaces (closer to perpendicular than not). **Video 3** of reconstructed ROI rotated for viewing from multiple angles corresponds to **D**, **F**, and **H**.

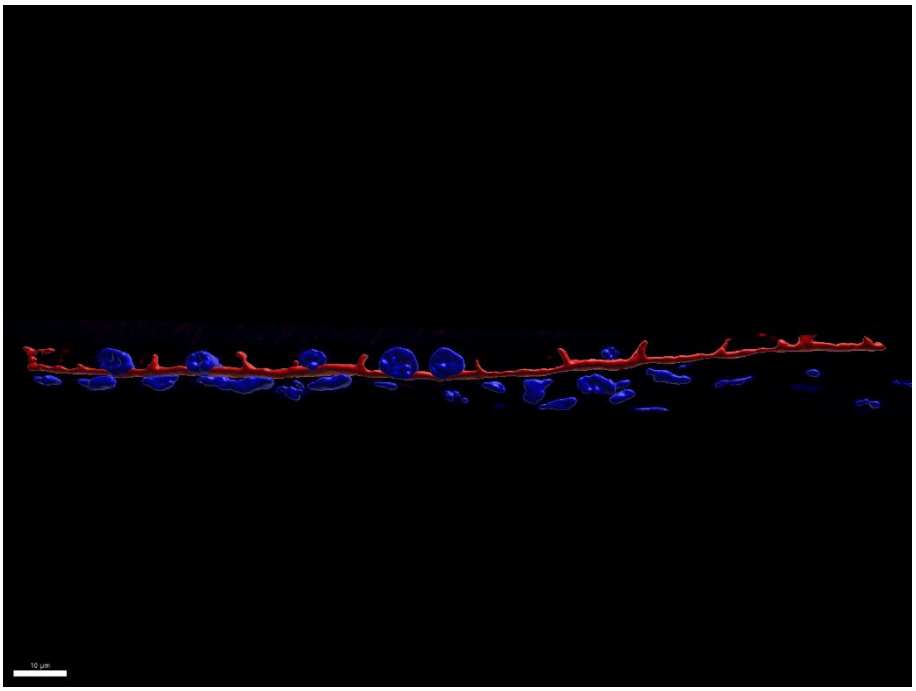

Video 3 – Rotation of 3D reconstruction selected from conventional cross sections for alternate angle viewing of lateral and basal face labeling.

Initially starts with single FOV highlighted in **Fig 2B** before zooming into selected ROI from **Fig 2C-H** and then rotated through 3D space. ROI is then widened to view entire lateral portion of RPE/choroid interface, highlighting differences in nuclear structure and position between RPE and underlying choriocapillaris.

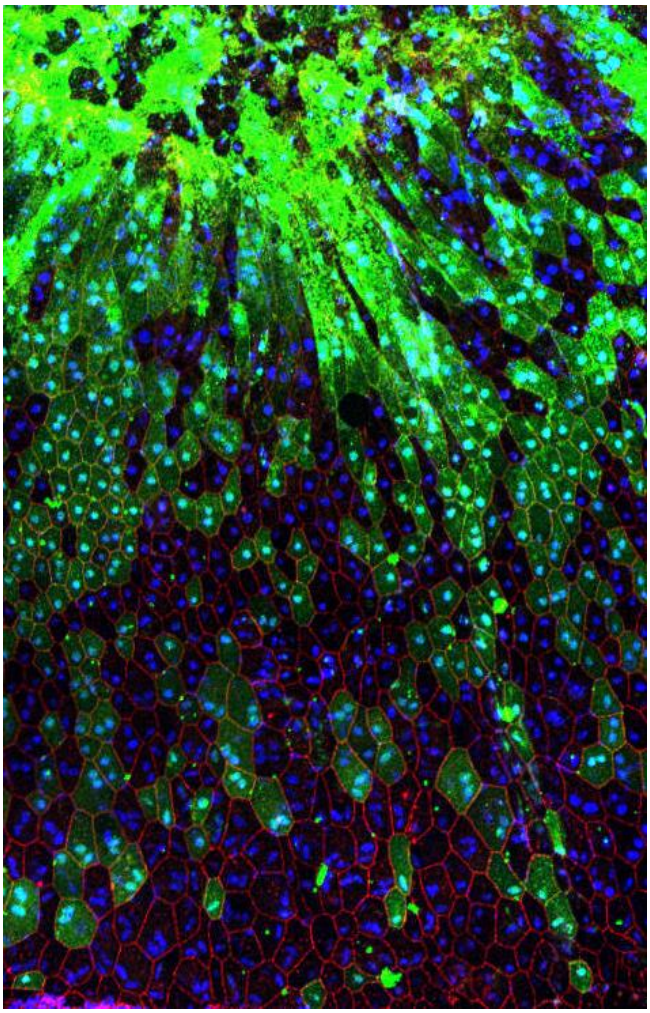

Figure 4 – ROI of "RPE-EMT" transitional region following NaIO3 administration.

Extremely high expression of ZsGreen linked to Best1 promoter activity is evident in regions where cell morphology is severely abnormal (bright green top 1/3 of image) and apical cell border delineation is non-existent (red, ZO-1) . Adjacent, intact cells are elongated before transitioning to more regular morphology further from the atrophic area.

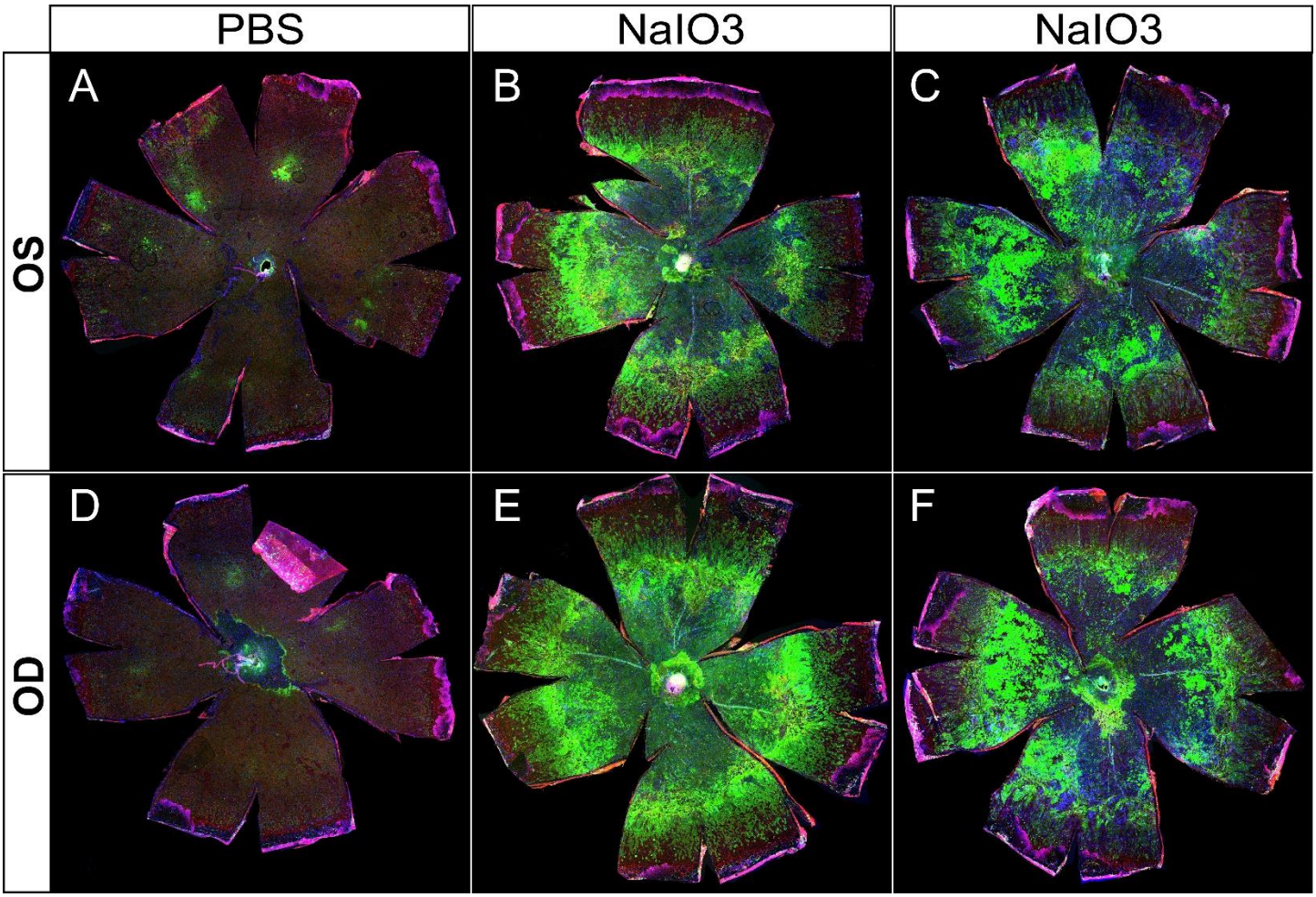

Figure 5 – Representative examples of whole-eye flatmounts prepared 8 days following control (PBS) or NaIO3 IP injections.

Drastically altered RPE morphology was observed in both eyes of animals following intravenous injection of NaIO3 (**B** and **E**, **C** and **F**) but not in those injected with only PBS vehicle (**A** and **D**). Of note is a general gradient of cellular stress severity, originating from the optic nerve head. A large central atrophic lesion is surrounded by a ring-like border region composed of cellular debris and aggregates (bright green = ZsGreen expression driven by Best1 promoter), most likely dying RPE cells. Continuing radially, an EMT-like response is seen characterized by elongation of RPE cells before transitioning to unaffected peripheral cells.